12. A. Nicholson, S. Frieda, A. Pearce, R. Silverstein, *Arterioscler. Thromb. Vasc. Biol.* **15**, 269 (1995).
13. G. Endemann *et al.*, *J. Biol. Chem.* **268**, 11811 (1993).
14. S. Nozaki *et al.*, *J. Clin. Invest.* **96**, 1859 (1995).
15. J. Savill, I. Dransfield, N. Hogg, C. Haslett, *Nature* **343**, 170 (1990).
16. J. Savill, N. Hogg, Y. Ren, C. Haslett, *J. Clin. Invest.* **90**, 1513 (1992).
17. Y. Ren, R. Silverstein, J. Allen, J. Savill, *J. Exp. Med.* **181**, 1857 (1995).
18. S. W. Ryeom, J. R. Sparrow, R. L. Silverstein, *J. Cell Sci.* **109**, 387 (1996).
19. K. Schneitz, P. Spielmann, M. Noll, *Genes Dev.* **7**, 114 (1993).
20. P. Heitzler, unpublished observations.
21. M. Boedigheimer and A. Laughon, *Development* **118**, 1291 (1993).
22. L. Frank and C. Rushlow, *ibid.* **122**, 1343 (1996).
23. Berkeley Drosophila Genome Project, unpublished data.
24. Single embryos were squished in 10 μl of 10 mM tris-HCl (pH8.0), 1 mM EDTA, and 25 mM NaCl containing Proteinase K (200 μg/ml; Boehringer Mannheim) and incubated at 37°C for 30 min, followed by 2 min at 95°C. The PCR was performed with 2.5 U of Taq polymerase and 100 ng of each primer. Two pairs of primers were designed to amplify 634 base pairs (bp) of the *crq* genomic sequence and 200 bp of the genomic region of the *doom* gene as an internal control [A. J. Harvey, A. P. Bidwaldi, L. K. Miller, *Mol. Cell. Biol.* **17**, 2835 (1997)]. *Crq*-specific primers were 5′-TGCCACCGATGCTTGCAGAT-3′ and 5′-AGCCGAATATGATTCCGTACTG-3′. *Doom*-specific primers were 5′-AGGGTAAACGGCCACAGAATGT-3′ and 5′-GATATCGTTGTAGTTGGCCCG-3′. The PCR cycles were 94°C for 1 min, 65°C for 1 min, and 72°C for 1 min for 30 cycles. In embryos from the *W88* stock, 20 of 79 were missing the *crq*-specific band.
25. CRQ immunostaining was used to genotype each embryo. Peroxidasin immunostaining detected all hemocytes [R. E. Nelson *et al.*, *EMBO J.* **13**, 3438 (1994)]. The nuclear dye 7-AAD labeled all DNA and allowed for the identification of apoptotic corpses. Unless otherwise specified, stage 11 to 16 embryos were fixed with standard procedures (*44*). Fixed devitellinized embryos were incubated in phosphate-buffered saline (PBS), 0.0125% saponin, 1% bovine serum albumin, and 4% normal goat serum (PSN) for 1 hour at room temperature and then incubated with the primary antibodies at a 1:1000 dilution in PSN overnight at 4°C. After several washes in PBS, the embryos were incubated for 1 hour at room temperature with the following secondary antibodies: fluorescein isothiocyanate–conjugated goat antibody to mouse and Cy5-conjugated goat antibody to rabbit (Jackson Immunoresearch) used at a 1:1000 dilution in PSN. Finally, embryos were washed three times in PBS for 20 min and subsequently incubated with 7-AAD (5 μg/ml) in PBS for 30 min. Embryos were quickly washed twice in PBS, mounted in Vectashield (Vector), and viewed by confocal microscopy (Leica TCS NT 4D).
26. The efficiency of engulfment was quantified by counting the number of engulfed corpses per macrophage in at least five fields of four embryos of each genotype. A P.I., that is, the mean number of engulfed corpses per macrophage, was calculated for each embryo, and the mean P.I. was derived for each genotype.
27. C. Phelps and A. Brand, *Methods* **14**, 367 (1998).
28. N. Franc and K. White, data not shown.
29. Stage 12 to 14 *w, UAS-crq;hs-Gal4/+* and control *w; hs-Gal4* embryos were heat-shocked for 1 hour at 39°C, aged for 2 hours at 25°C, and fixed and embedded in Spurr's resin (*34*). Serial 1-μm sections of two embryos of each genotype were stained with a solution of methylene, toluidine blue, and borax (*44*) and viewed by standard microscopy.
30. J. Pugin *et al.*, *Immunity* **1**, 509 (1994).
31. A. Devitt *et al.*, *Nature* **392**, 505 (1998).
32. Stage 11 embryos were microinjected with a solution of PBS and 2 mM NaN_3 containing about 6×10^8 tetramethyl rhodamine isothiocyanate (TRITC)–labeled fluorescent *E. coli* (K-12 strain) or *S. aureus* (Wood strain) bioparticles (heat-killed bacteria; Molecular Probes) with standard microinjection procedures (*44*). After injection, embryos were kept in the dark at 18°C for 14 to 16 hours, incubated for 1 hour at 4°C, mounted, and viewed under Nomarski and fluorescence with a confocal microscope.
33. J. Abrams, A. Lux, H. Steller, M. Krieger, *Proc. Natl. Acad. Sci. U.S.A.* **89**, 10375 (1992).
34. K. White *et al.*, *Science* **264**, 677 (1994).
35. M. E. Grether, J. M. Abrams, J. Agapite, K. White, H. Steller, *Genes Dev.* **9**, 1694 (1995).
36. P. Chen, W. Nordstrom, B. Gish, J. M. Abrams, *ibid.* **10**, 1773 (1996).
37. After CRQ immunostaining, the amount of fluorescence seen in five isolated macrophages of each genotype was quantified with a confocal microscope. For each macrophage, the fluorescence of serial sections of 0.5 μm was quantified from top to bottom of the cell. After subtracting the background fluorescence, the total amount of fluorescence within each macrophage was calculated.
38. M. Hortsch *et al.*, *Int. J. Dev. Biol.* **42**, 33 (1998).
39. J.-L. Dimarcq *et al.*, *Insect Biochem. Mol. Biol.* **27**, 877 (1997).
40. E. Gateff *et al.*, in *Invertebrate Systems In Vitro*, E. Kurstak, K. Maramorosch, A. Dubendorfer, Eds. (North-Holland, Elsevier, Amsterdam, 1980), pp. 517–533.
41. L. Nagy, P. Tontonoz, J. Alverez, H. Chen, R. Evans, *Cell* **93**, 229 (1998).
42. A. Pearson, A. Lux, M. Krieger, *Proc. Natl. Acad. Sci. U.S.A.* **92**, 4056 (1995).
43. V. Rodrigues, P. Cheah, K. Ray, W. Chia, *EMBO J.* **14**, 3007 (1995).
44. M. Ashburner, Drosophila: *A Laboratory Manual* (Cold Spring Harbor Laboratory Press, Cold Spring Harbor, NY, 1989).
45. We thank J. Fessler and M. Hortsch for providing antibodies; E. Noll, N. Perrimon, the Bloomington Stock Center, and L. Dobens for fly stocks; M. Krieger for the DiI AcLDLs; Y. Ge and W. Fowle for assistance with confocal microscopy and histology; the lab of T. Orr-Weaver for advice on nuclear dyes; I. Ando for suggesting the bacteria assay experiment; and J. Settleman and the members of the Ezekowitz and White laboratories for helpful comments on this work. This work was supported by grants from the Shiseido Company of Japan to Massachusetts General Hospital/Harvard Medical School (N.C.F. and K.W.), from NIH (K.W. and A.E.), and from the Human Frontiers in Science Program (A.E. and N.C.F.).

5 February 1999; accepted 12 May 1999

Vessel Cooption, Regression, and Growth in Tumors Mediated by Angiopoietins and VEGF

J. Holash,[1] P. C. Maisonpierre,[1] D. Compton,[1] P. Boland,[1] C. R. Alexander,[1] D. Zagzag,[2] G. D. Yancopoulos,[1]* S. J. Wiegand[1]*

In contrast with the prevailing view that most tumors and metastases begin as avascular masses, evidence is presented here that a subset of tumors instead initially grows by coopting existing host vessels. This coopted host vasculature does not immediately undergo angiogenesis to support the tumor but instead regresses, leading to a secondarily avascular tumor and massive tumor cell loss. Ultimately, however, the remaining tumor is rescued by robust angiogenesis at the tumor margin. The expression patterns of the angiogenic antagonist angiopoietin-2 and of pro-angiogenic vascular endothelial growth factor (VEGF) suggest that these proteins may be critical regulators of this balance between vascular regression and growth.

It is widely accepted that most tumors and metastases originate as small avascular masses that belatedly induce the development of new blood vessels once they grow to a few millimeters in size (*1–3*). Initial avascular growth would be predicted for tumors that arise in epithelial structures that are separated from the underlying vasculature by a basement membrane and for experimental tumors that are implanted into avascular settings (such as the cornea pocket) or into a virtual space (such as the subcutaneum) (*2*, *3*). However, there is also evidence to suggest that tumors in more natural settings do not always originate avascularly, particularly when they arise within or metastasize to vascularized tissue (*4*). In such settings, tumor cells may coopt existing blood vessels (*4*). The interplay between this coopting of existing vessels and subsequent tumor-induced angiogenesis has not been extensively examined nor has the role of angiogenic factors in this process.

The pro-angiogenic vascular endothelial growth factors (VEGFs) and the angiopoietins are the only known growth factor families that are specific for the vascular endothelium because expression of their receptors is restricted to these cells (*5*, *6*). The angiopoietins include both receptor activators [angiopoietin-1 (Ang-1)] and receptor antagonists [angiopoietin-2

[1]Regeneron Pharmaceuticals, 777 Old Saw Mill River Road, Tarrytown, NY 10591, USA. [2]Microvascular and Molecular Neuro-Oncology Laboratory, Department of Pathology, Kaplan Cancer Center, New York University Medical Center, New York, NY 10016, USA.

*To whom correspondence should be addressed. E-mail: gdy@regpha.com (G.D.Y.); stan.wiegand@regpha.com (S.J.W.)

(Ang-2)] (*7–10*). The VEGFs and the angiopoietins seem to play complementary and coordinated roles in vascular development (*9*, *11*). During development, VEGF acts via the Flk1/KDR receptor to promote endothelial cell differentiation, proliferation, and primitive vessel formation (*12*). Ang-1 subsequently acts via the Tie2 receptor to remodel these primitive vessels and is then thought to help maintain and stabilize the mature vessels by promoting interactions between endothelial cells and surrounding support cells (*6–9*, *11*, *13*, *14*). In adults, Ang-2 is expressed primarily at sites of vascular remodeling (*9*, *11*), where it is thought to block the constitutive stabilizing action of Ang-1. It has been proposed that destabilization by Ang-2 in the absence of VEGF leads to frank vessel regression, whereas such destabilization in the presence of high VEGF levels facilitates the angiogenic response (*9*, *11*). In tumors, hypoxia-induced VEGF (*15*) apparently recapitulates its developmental actions by contributing to the onset of tumor-associated angiogenesis, and antagonists of VEGF have been shown to inhibit the growth of many tumors (*16*).

To explore the possibility that VEGFs and angiopoietins collaborate during tumor angiogenesis, we studied early angiogenic events using the rat C6 glioma model (*17*). Remarkably, even the smallest C6 gliomas at just 1 week after implantation (<1 mm in diameter) were found to be well vascularized (Fig. 1, A and A′). As previously noted (*17*), this is attributable to the coopting of existing brain blood vessels by the implanted tumor cells. The vessels within these early tumors were similar to normal brain vessels in caliber and heterogeneity. There was no evidence of angiogenesis, as judged by the lack of vascular sprouts, noncanalized endothelial cell chains, and hyperplastic vessels. By 2 weeks after implantation, the tumors had grown to ≥2 mm in diameter but still showed no obvious angiogenic response. Rather, they exhibited a dramatic decrease in vessel density, presumably due to tumor growth in the absence of compensatory angiogenesis (Fig. 1, B and B′). The vessels within the tumors were distinctly larger and more homogeneous in caliber than the microvasculature of the normal brain. By 4 weeks after implantation, the tumors measured several millimeters in diameter and showed marked changes in comparison with tumors at earlier stages of development (Fig. 1, C and C′). Blood vessels within the core of the tumor had undergone dramatic regression, with no evidence of a local, compensatory angiogenic response. The centers of the tumors were largely bereft of vessels, leading to massive tumor cell death (Fig. 1, C and C′). The remaining cells in the tumor interior were organized in cuffs of pseudopalisading cells around the few surviving internal vessels (Fig. 1, C and C′). In contrast to the tumor interior, the tumor periphery displayed robust angiogenesis (Fig. 1, C and C′).

Regression of coopted blood vessels was a very early event that preceded tumor cell death. Apoptotic cells were predominantly found in blood vessels in early-stage tumors, whereas at later stages there was widespread apoptosis of tumor cells (Fig. 2, A through C). Staining with markers for both endothelial cells and supporting pericytes or smooth muscle cells revealed that vessel regression was associated with progressive disengagement of endothelial cells from surrounding support cells (Fig. 1, D through G).

The apparent association of tumor vessel regression, apoptosis, and disruption of endothelial cell interactions with support cells raised the possibility that blockade of the stabilizing action of Ang-1 might be contributing to tumor vessel regression. Consistent with this possibil-

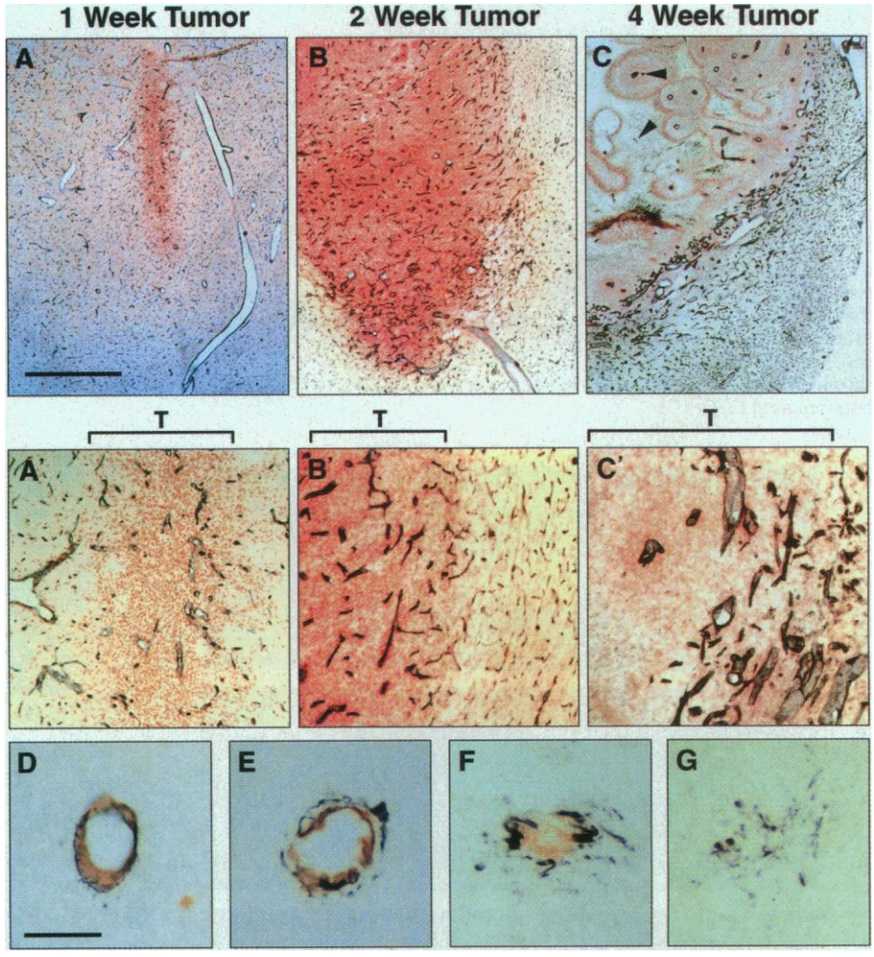

Fig. 1. Sections from rat C6 gliomas (*28*) showing progressive vessel regression, accompanied by dissociation of endothelial and smooth muscle cells. (**A** and **A′**) Small 1-week tumors that measure a fraction of a millimeter in width are well vascularized as determined by RECA immunostaining (*29*), apparently because they coopt and grow around existing vessels. [T, tumor; scale bar in (A), 1 mm for (A) through (C) and 200 μm for (A′) through (C′)] The vessels in early tumors resemble vessels in surrounding brain tissue in both density and morphology. (**B** and **B′**) Two-week tumors continue to have extensive internal vasculature, although the vessel density is less than that in surrounding brain tissue, presumably because of the growth of the tumor in the absence of compensatory angiogenesis from existing internal vessels; the caliber of the internal vessels within these tumors does become dilated and relatively uniform compared to normal brain vessels. (**C** and **C′**) Within large 4-week tumors, internal vessels regress with accompanying loss of surrounding tumor (necrotic tumor areas are unstained). Surviving internal vessels are sparse and uniform, are centrally located with respect to surrounding cuffs of well-stained viable tumor cells, and exhibit no evidence of compensatory angiogenesis; although robust angiogenesis is apparent at the margin of the tumor, where increased density of ectatic vessels is noted. Arrowheads in (C) depict a patent (top) and a regressed (bottom) vessel, each surrounded by either a surviving or regressed cuff of tumor. (**D** through **G**) Immunostaining with antibodies to SMA (black) and RECA (brown) (*29*) shows that pericytes and smooth muscle cells detach from the vessel wall in tumors. (D) shows a vessel wall in normal brain tissue in which RECA and SMA staining are essentially superimposed, whereas (E) through (G) depict vessels within tumors with progressive detachment of SMA-positive cells and vessel regression. Scale bar in (D) indicates 50 μm for (D) through (G).

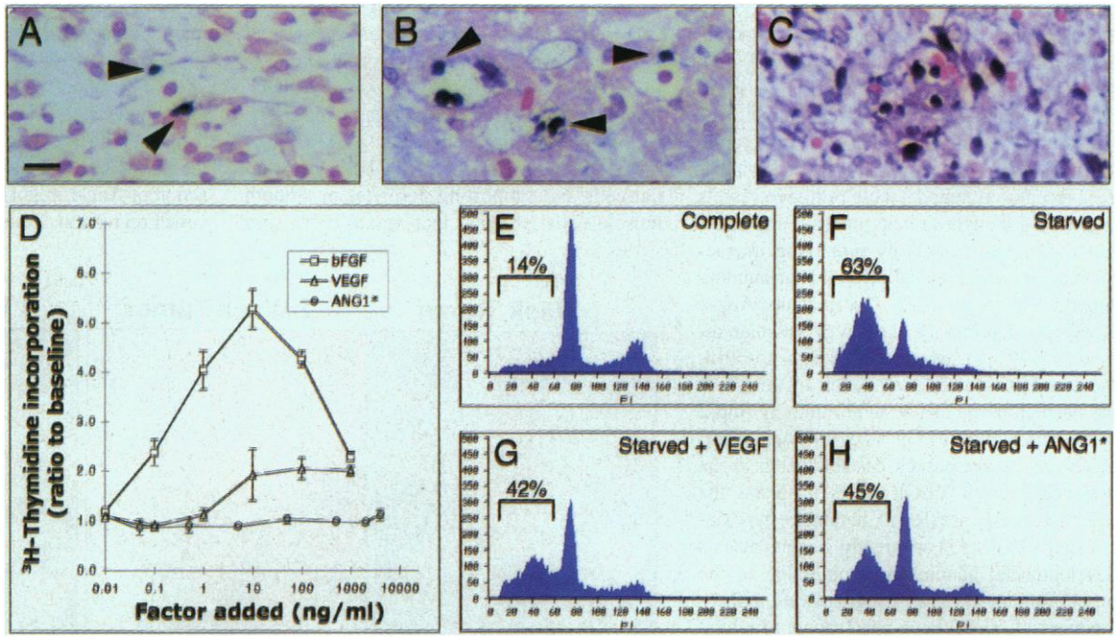

Fig. 2. Detection of apoptosis in rat C6 gliomas. Vessel-specific apoptosis (*25*, *29*) is evident in early tumors (**A** and **B**), and this is followed by widespread apoptosis of tumor cells at later stages (**C**); arrowheads denote vessel-specific apoptotic figures (stained black) in panels. Scale bar in (A), 10 μm. Flow cytometry experiments (**E** through **H**) indicate that Ang-1 can be as effective as VEGF in preventing apoptosis of serum-starved endothelial cells, as judged by a decreased percentage of endothelial cells with hypodiploid DNA content (see percentages over the sub-G_0/G_1 peak delineated by brackets). Cell number is shown on the *y* axis. PI, propidium iodide. However, in contrast to VEGF, Ang-1 cannot promote DNA synthesis in these cells (**D**) (*30*). Similar data have just been reported (*31*).

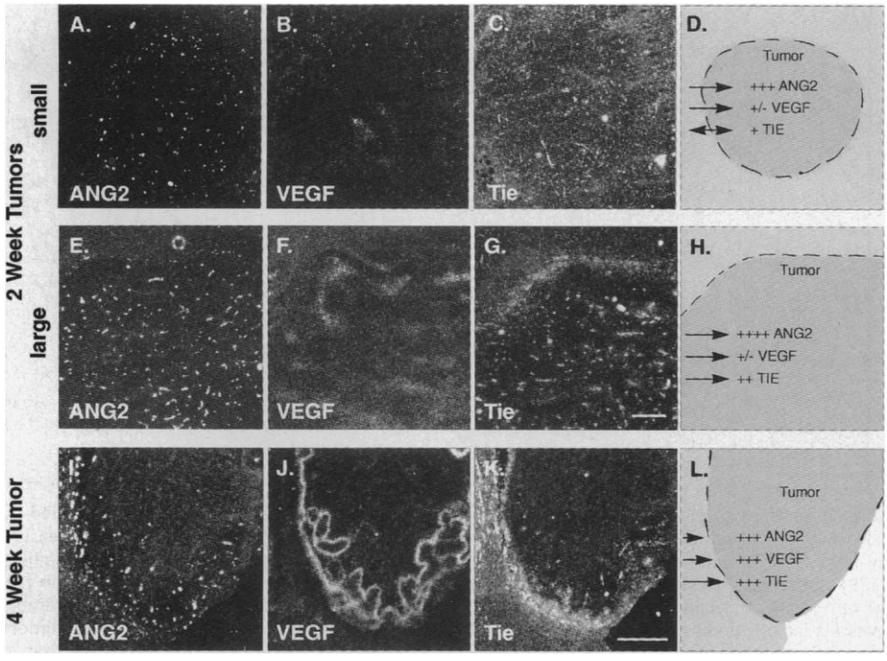

Fig. 3. In situ hybridization analysis of Ang-2, VEGF, and Tie mRNA in two different 2-week rat gliomas (small and large) and a large 4-week rat glioma (*29*, *32*). At 2 weeks, the vessels within both a small tumor (**A** through **D**) and a larger tumor (**E** through **H**) consistently express high levels of Ang-2 mRNA (A and E). In contrast, up-regulation of Tie mRNA (C and K) is restricted to the larger tumor. Induction of VEGF is minimal in small tumors (B) and is still modest and patchy in larger tumors (F). In very large 4-week tumors, the tumor is secondarily avascular because of massive vessel regression and thus has few internal vessels, but has a hypervascular plexus at the tumor border. The few internal and the many rim vessels are now marked by both Ang-2 and Tie (**I** and **K**), although expression of Ang-2 is more punctate than that of Tie. The remaining live tumor cuffs around vessels show dramatically up-regulated VEGF expression (**J**). This VEGF expression is highest in palisading, presumably hypoxic, tumor cells that are furthest from vessels; large areas within the tumor, between palisading cells, are necrotic. (D), (H), and (L) outline the boundaries of the tumor within the brain and indicate the relative levels of expression of Ang-2, VEGF, and Tie. Scale bar in (G) indicates 500 μm for (A) through (H); scale bar in (K) indicates 1 mm for (I) through (L).

ity, Ang-1 was found to be anti-apoptotic for cultured endothelial cells (Fig. 2, E through H), and expression of its antagonist, Ang-2, was found to be induced in the endothelium of coopted tumor vessels before their regression (Fig. 3A). In contrast, marked induction of VEGF expression occurred much later in tumor progression, in the hypoxic periphery of tumor cells surrounding the few remaining internal vessels, as well as adjacent to the robust plexus of vessels at the tumor margin (Fig. 3, B, F, and J). Expression of Ang-2 continued to mark not only the few surviving internal vessels but also the angiogenic vessels at the tumor margin (Fig. 3I), which suggests that the destabilizing action of Ang-2 facilitates the angiogenic action of VEGF at the tumor rim. Ang-1 expression did not change significantly throughout tumor development. Consistent with its expression in C6 glioma cells in culture (*18*), in relatively small tumors Ang-1 mRNA was expressed in a diffuse pattern by the tumor cells themselves (*19*) at levels just above that in the normal brain. Unlike VEGF, Ang-1 was not expressed at elevated levels in hypoxic regions of large tumors (*20*–*22*).

We also examined human glioblastomas (*20*, *21*). Ang-2 was not detectable in the normal human brain, but its expression was dramatically induced in coopted tumor vessels, preceding vessel regression. As in the rat C6 model, this occurred in association with a disruption of interactions between endothelial and smooth muscle cells and with endothelial cell apoptosis. Diffuse Ang-1 expression in the human tumors also resembled that seen in the rat model (*20*–*22*).

To examine whether these findings are generalizable to other tumor types, we implanted rat RBA mammary adenocarcinoma cells into rat brains. Rather than growing avascularly, the implanted RBA cells rapidly associated with and migrated along cerebral blood vessels in a manner even more striking than that observed with the glioma cells (Fig. 4, A and D). Consistent with the well-vascularized state of these early tumors, there was minimal up-regulation of VEGF (*22*). However, the coopted vessels displayed striking and specific up-regulation of Ang-2, which was not detectable in the vessels of adjacent brain tissue (Fig. 4B). Preliminary analysis of RBA tumors at a later stage indicated that Ang-2 expression was associated with a pattern of vascular regression (in the absence of VEGF) and angiogenesis (in the presence of VEGF), as was the case with gliomas (*22*). Ang-1 was not expressed in cultured RBA cells or the tumors themselves (*22*).

Examination of a model of tumor metastasis, in which the mouse lung is colonized by intravenously injected Lewis lung carcinoma cells, yielded similar results. Tiny tumor metastases (arrowheads, Fig. 4, E and F) as well as moderately sized tumor nodules (arrows, Fig. 4, E and F) were closely associated with pulmonary vessels, and these vessels showed dramatic induction of Ang-2 expression (Fig. 4F). Progressively larger tumor nodules appeared to be characterized by vessel regression as well as neo-angiogenesis, again correlating with Ang-2 and VEGF expression (*22*).

In summary, our analyses of several different tumor models suggest a modification of the prevailing view that most malignancies and metastases originate as avascular masses that only belatedly induce angiogenic support. Our findings indicate that a subset of tumors rapidly coopts existing host vessels to form an initially well-vascularized tumor mass. Perhaps as part of a host defense mechanism, there is widespread regression of these initially coopted vessels, leading to a secondarily avascular tumor and massive tumor cell loss; however, the remaining tumor is ultimately rescued by robust angiogenesis at the tumor margin.

The expression patterns of VEGF and the natural Tie2 receptor antagonist Ang-2 strongly implicate them in these processes. There is a striking induction of Ang-2 expression in coopted vessels before induction of VEGF expression in the adjacent tumor cells, providing perhaps the earliest marker of tumor vasculature. The intense autocrine expression of Ang-2 by endothelial cells in tumor-associated vessels may counter a paracrine stabilization or survival signal provided by low-level constitutive expression of Ang-1 in normal tissues. We hypothesize that Ang-2 "marks" the coopted vessels for regression by an apoptotic mechanism that may involve disrupted interactions between endothelial cells and the surrounding extracellular matrix and supporting cells. Subsequently, VEGF up-regulation coincident with Ang-2 expression at the tumor periphery is associated with robust angiogenesis. This late expression of tumor-derived VEGF may nullify the regression signal provided by Ang-2, which is consistent with the observation that VEGF is required for tumor vessel survival (*23*).

The angiogenic properties of tumor-derived VEGF may actually be facilitated when vessels are destabilized by Ang-2. Newly formed tumor vessels are often tenuous, poorly differentiated, and undergo regressive changes even as blood vessel proliferation continues. The failure of many solid tumors to form a well-differentiated and stable vasculature may be attributable to the fact that newly formed tumor vessels continue to overexpress Ang-2. In fact, hypervascular hepatomas with aberrant vasculatures show high levels of Ang-2 expression in their endothelium (*24*). Thus, a persistent blockade of Tie2 signaling, which is otherwise constitutively activated in many normal adult tissues (*14*), may prevent tumor vessel differentiation and maturation and contribute to their generally tenuous and leaky nature.

In tumors, Ang-2 and VEGF apparently reprise the roles they play during vascular remodeling in normal tissues, acting to regulate the previously underappreciated balance between vascular regression and growth. Our findings bolster the case for anti-VEGF therapies in cancer, not only to prevent further angiogenesis but also perhaps to promote the regression of fragile new tumor vessels. Ang-2 appears to be the earliest marker of blood vessels that have been perturbed by invading tumor cells. As such, Ang-2 may prove to be useful in the imaging of very

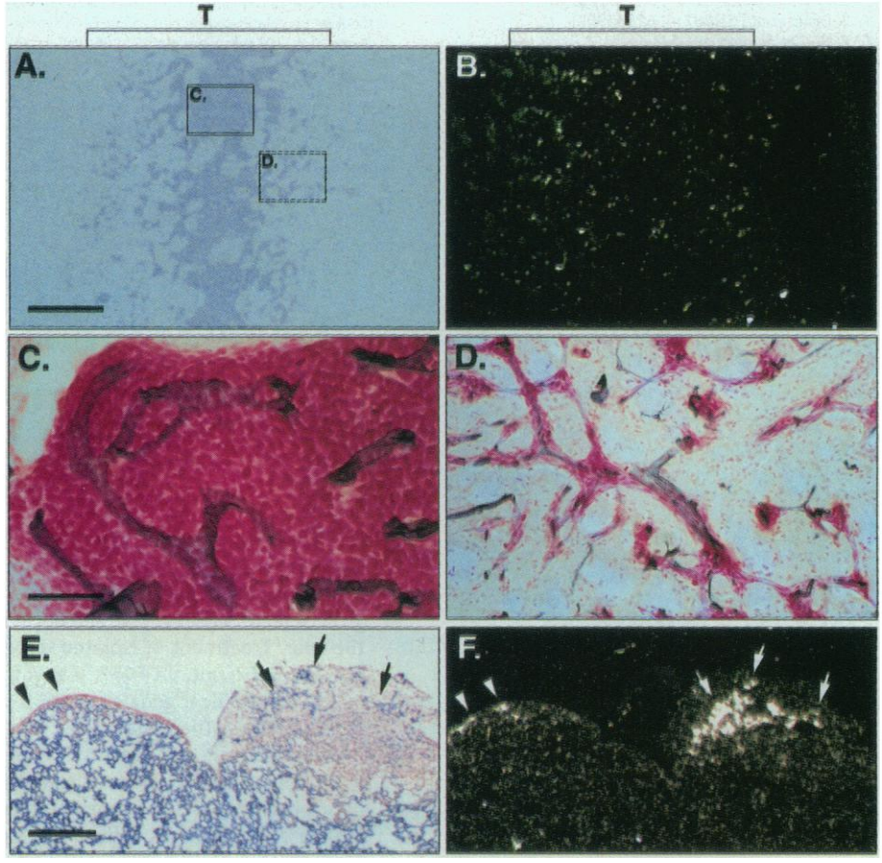

Fig. 4. In situ hybridization analysis (*32*) of rat RBA mammary carcinomas (*28*) and mouse Lewis lung carcinomas (*28*), showing up-regulation of Ang-2 mRNA in coopted tumor vessels. (**A**) A section through a mammary carcinoma stained with cresyl violet demonstrates the invasiveness of the tumor cells in the brain. The boxes within (A) delineate regions of the tumor core and periphery. Similar regions in specimens stained with an antibody to RECA (*29*) are shown in (**C**) and (**D**). The dramatic homing of tumor cells to blood vessels is especially apparent in (D). (**B**) Whereas VEGF is typically weak or undetectable at this tumor stage (*22*), Ang-2 is highly expressed in a punctate manner by blood vessels. (**E**) A section through a Lewis lung carcinoma stained with Pyronin Y demonstrates a metastasis only a few cells thick (left, arrowheads) and a slightly larger metastasis (right, arrows). Vessels, stained black with antibodies to PECAM (*29*), lie within these small tumors. (**F**) The vessels coopted by the small Lewis lung metastases exhibit dramatic induction of Ang-2. Scale bar in (A) indicates 500 μm for (A) and (B); scale bar in (C) indicates 25 μm for (C) and 50 μm for (D); scale bar in (E) indicates 500 μm for (E) and (F).

small tumors and metastases and possibly in schemes designed to specifically target chemotoxic therapy to tumor vasculature.

References and Notes

1. J. Folkman, *N. Engl. J. Med.* **285**, 1182 (1971).
2. ———, *J. Natl. Cancer Inst.* **82**, 4 (1990).
3. D. Hanahan and J. Folkman, *Cell* **86**, 353 (1996).
4. P. Wesseling, J. A. van der Laak, H. de Leeuw, D. J. Ruiter, P. C. Burger, *J. Neurosurg.* **81**, 902 (1994); L. Holmgren, M. S. O'Reilly, J. Folkman, *Nature Med.* **1**, 149 (1995); F. Pezzella, *et al.*, *Am. J. Pathol.* **151**, 1417 (1997).
5. D. J. Dumont, T. P. Yamaguchi, R. A. Conlon, J. Rossant, M. L. Breitman, *Oncogene* **7**, 1471 (1992); J. Partanen *et al.*, *Mol. Cell. Biol.* **12**, 1698 (1992); A. Iwama *et al.*, *Biochem. Biophys. Res. Commun.* **195**, 301 (1993); P. C. Maisonpierre, M. Goldfarb, G. D. Yancopoulos, G. Gao, *Oncogene* **8**, 1631 (1993); T. N. Sato, Y. Qin, C. A. Kozak, K. L. Audus, *Proc. Natl. Acad. Sci. U.S.A.* **90**, 9355 (1993); H. Schnurch and W. Risau, *Development* **119**, 957 (1993); S. F. Ziegler, T. A. Bird, S. A. Schneringer, K. A. Schooley, P. R. Baum, *Oncogene* **8**, 663 (1993); N. Ferrara, *Curr. Top. Microbiol. Immunol.* **237**, 1 (1999).
6. D. J. Dumont *et al.*, *Genes Dev.* **8**, 1897 (1994); T. N. Sato *et al.*, *Nature* **376**, 70 (1995).
7. S. Davis *et al.*, *Cell* **87**, 1161 (1996).
8. C. Suri *et al.*, *ibid.*, p. 1171.
9. P. C. Maisonpierre *et al.*, *Science* **277**, 55 (1997).
10. D. Valenzuela *et al.*, *Proc. Natl. Acad. Sci. U.S.A.* **96**, 1904 (1999).
11. A diagram depicting the complementary and coordinated roles of VEGF and the angiopoietins during vascular growth and development can be found at *Science* Online (Web Fig. 1 at www.sciencemag.org/feature/data/1039904.shl).
12. F. Shalaby *et al.*, *Nature* **376**, 62 (1995); P. Carmeliet *et al.*, *ibid.* **380**, 435 (1996); N. Ferrara *et al.*, *ibid.*, p. 439.
13. C. Suri *et al.*, *Science* **282**, 468 (1998).
14. A. Wong *et al.*, *Circ. Res.* **81**, 567 (1997).
15. D. Shweiki, M. Neeman, A. Itin, E. Keshet, *Proc. Natl. Acad. Sci. U.S.A.* **92**, 768 (1995).
16. K. J. Kim *et al.*, *Nature* **362**, 841 (1993); B. Millauer, L. K. Shawver, K. H. Plate, W. Risau, A. Ullrich, *ibid.* **367**, 576 (1994); R. S. Warren, H. Yuan, M. R. Matli, N. A. Gillett, N. Ferrara, *J. Clin. Invest.* **95**, 1789 (1995); B. Millauer *et al.*, *Cancer Res.* **56**, 1615 (1996); C. K. Goldman *et al.*, *Proc. Natl. Acad. Sci. U.S.A.* **95**, 8795 (1998).
17. N. Nagano, H. Sasaki, M. Aoyagi, K. Hirakawa, *Acta Neuropathol.* **86**, 117 (1993).
18. B. Enholm *et al.*, *Oncogene* **14**, 2475 (1997).
19. A figure showing the expression patterns of Tie1, Tie2, Ang-1, Ang-2, and VEGF in early rat C6 gliomas can be found at *Science* Online (Web Fig. 2 at www.sciencemag.org/feature/data/1039904.shl).
20. A. Stratmann, W. Risau, K. H. Plate, *Am. J. Pathol.* **153**, 1459 (1998).
21. A complete description of angiopoietin expression in human glioblastomas can be found at *Science* Online (Web Fig. 3 at www.sciencemag.org/feature/data/1039904.shl); D. Zagzag *et al.*, *Exp. Neurol.*, in press.
22. J. Holash *et al.*, unpublished observations; D. Zagzag *et al.*, unpublished observations.
23. L. Benjamin, D. Golijanin, A. Itin, D. Pode, E. Keshet, *J. Clin. Invest.* **103**, 159 (1999).
24. S. Tanaka *et al.*, *ibid.*, p. 341.
25. S. D. Morgenbesser *et al.*, *EMBO J.* **14**, 743 (1995).
26. J. K. Morse *et al.*, *J. Neurosci.* **13**, 4146 (1993).
27. D. M. Valenzuela *et al.*, *Neuron* **10**, 963 (1993).
28. Tumor cells were obtained from the American Type Culture Collection and grown in culture. About 1.0×10^5 C6 or RBA cells were suspended in ~2 μl of phosphate-buffered saline (PBS) and injected stereotaxically over a period of 5 to 10 min into the right striatum (AP + 0.5; ML −3.0; DV −6.0 relative to Bregma) of adult male Sprague-Dawley rats. About 5.0×10^5 Lewis lung carcinoma cells were suspended in 50 μl of serum-free media and injected into the jugular vein of adult male C57Bl mice.
29. Animals were anesthetized and either decapitated or perfused with 4% paraformaldehyde. Brains for thick sliding microtome sections (40 μm) were post-fixed in 4% paraformaldehyde overnight and then equilibrated in 35% sucrose. Fixed brains for thin sections (10 μm) were equilibrated in 17% sucrose. Fixed and fresh brains were frozen in methylbutane, chilled in dry ice, and sectioned on a cryostat. For TUNEL labeling (*25*), brains were immersion-fixed in 10% neutral buffered formalin and embedded in paraffin. Fixed sections were immunostained with a monoclonal antibody to rat endothelial cell antigen (RECA1; 1:250; Serotec) and a biotinylated horse anti-mouse secondary antibody (1:1500; Vector) or with a monoclonal antibody to PECAM (CD31; 1:100; Pharmingen) and a biotinylated rabbit anti-rat secondary antibody (1:150; Vector) as previously described (*26*). A similar protocol was used for double labeling. Sections were initially labeled with a monoclonal antibody to alpha smooth muscle actin (SMA; 1:500; DAKO) and a biotinylated goat anti-mouse immunoglobulin G IIa secondary antibody (1:1250; Amersham). SMA staining was visualized with a Vectastain Elite kit (Vector), and a black reaction product was generated by nickel sulfate enhancement. After SMA labeling, sections were then reblocked and labeled with antibody to RECA (1:100). A brown reaction product was used.
30. Human umbilical vein endothelial cells (HUVECs) (Clonetics, San Diego, CA) were maintained in recommended medium on gelatin-coated plastic. For DNA synthesis assays, 1×10^4 cells were plated in 96-well microwells and grown for 24 hours in basal medium plus 0.5% fetal bovine serum. Cells were re-fed with the same medium plus purified factors and grown for 20 hours, with 1 mCi tritiated thymidine (80 Ci/mmol; Amersham) being present for the last 3 hours of incubation. Cells were rinsed and fixed with trichloroacetic acid, and thymidine incorporation was measured by standard liquid scintillation techniques. Ang-1* (ANG1*) was a modified form of human Ang-1, described previously (*9*); VEGF was murine VEGF-164, produced and purified from baculovirus-infected insect cells; bFGF was human basic fibroblast growth factor (R&D Systems). For assessing resistance to apoptosis, plates of ~80% confluent HUVECs were rinsed twice with basal medium and grown for 18 to 20 hours in basal medium and bovine serum albumin (0.5 mg/ml), plus or minus purified factors. Both adherent and nonadherent cells were harvested, pooled, and fixed in 70% ethanol at −20°C overnight. Cells were washed in PBS, incubated for 30 min with ribonuclease A (5 kunitz units/ml; Sigma) and propidium iodide (50 μg/ml; Sigma). Cellular DNA content, as judged by propidium iodide fluorescence, was measured by flow cytometry (MoFlo, Cytomation, Fort Collins, CO).
31. A. Papapetropoulos *et al.*, *Lab. Invest.* **79**, 213 (1999).
32. Fresh frozen or fixed sections were probed with ^{35}S-labeled cRNAs (*27*). Probes for VEGF and Ang-1 and Ang-2 have been described (*9*). For Tie1, a 1.3-kb fragment of rat Tie1 spanning the last 309 codons and 375 base pairs of the 3′ untranslated sequence was used, and for Tie2 a 460–base pair fragment spanning codons 771 through 924 within the kinase domain was used. This probe does not cross-hybridize to Tie1 mRNA in Northern blots.

33. We thank B. Luan, J. Zheng, P. Burfeind, S. Zabski, and F. Martin for excellent technical assistance; E. Burrows and C. Murphy for graphics work; A. Hooper and D. Friedlander for data on human gliomas; and M. Grumet for intellectual discussions. Supported in part by a grant from the Children's Brain Tumor Foundation to D.Z. and by Procter & Gamble Pharmaceuticals, Inc. All animal studies were done in accordance with institutional guidelines.

9 March 1999; accepted 10 May 1999

Initiation of Mammalian Liver Development from Endoderm by Fibroblast Growth Factors

Joonil Jung,[1] Minghua Zheng,[1] Mitchell Goldfarb,[2] Kenneth S. Zaret[1]*

The signaling molecules that elicit embryonic induction of the liver from the mammalian gut endoderm or induction of other gut-derived organs are unknown. Close proximity of cardiac mesoderm, which expresses fibroblast growth factors (FGFs) 1, 2, and 8, causes the foregut endoderm to develop into the liver. Treatment of isolated foregut endoderm from mouse embryos with FGF1 or FGF2, but not FGF8, was sufficient to replace cardiac mesoderm as an inducer of the liver gene expression program, the latter being the first step of hepatogenesis. The hepatogenic response was restricted to endoderm tissue, which selectively coexpresses FGF receptors 1 and 4. Further studies with FGFs and their specific inhibitors showed that FGF8 contributes to the morphogenetic outgrowth of the hepatic endoderm. Thus, different FGF signals appear to initiate distinct phases of liver development during mammalian organogenesis.

Identifying the molecular signals that initiate organogenesis from the gut is important for understanding the fundamental mechanisms of developmental regulation, hereditary digestive disorders, and tissue regeneration. Different segments of the mammalian gut endoderm give rise to the liver, lung, pancreas, thyroid, and gastrointestinal tract. Typically, a portion of the endoderm will begin to express genes specific to one of these tissues, and then the newly specified cells will proliferate out of the endoderm layer to form a tissue bud, initiating morphogenesis (*1, 2*). In *Drosophila*, the initial specification of tissues

[1]Department of Molecular Biology, Cell Biology, and Biochemistry, Brown University, Box G-J363, Providence, RI 02912, USA. [2]Brookdale Center for Molecular Biology, Mount Sinai School of Medicine, New York, NY 10029, USA.

*To whom correspondence should be addressed: E-mail: zaret@brown.edu